Biol. Cybern. 90, 59–74 (2004)
DOI 10.1007/s00422-003-0447-1

Biological Cybernetics

Intrinsic bursting activity in the pre-Bötzinger Complex: Role of persistent sodium and potassium currents

Ilya A. Rybak[1], **Natalia A. Shevtsova**[1], **Krzysztof Ptak**[2], **Donald R. McCrimmon**[2]

[1] School of Biomedical Engineering, Science and Health Systems, Drexel University, Philadelphia, PA 19104, USA
[2] Department of Physiology and Institute for Neuroscience, Feinberg School of Medicine, Northwestern University, Chicago, IL 60611-3008, USA

Received: 14 April 2003 / Accepted: 24 September 2003 / Published online: 21 January 2004

Abstract. Computational models of single pacemaker neuron and neural population in the pre-Bötzinger Complex (pBC) were developed based on the previous models by Butera et al. (1999a,b). Our modeling study focused on the conditions that could define endogenous bursting vs. tonic activity in single pacemaker neurons and population bursting vs. asynchronous firing in populations of pacemaker neurons. We show that both bursting activity in single pacemaker neurons and population bursting activity may be released or suppressed depending on the expression of persistent sodium (I_{NaP}) and delayed-rectifier potassium (I_K) currents. Specifically, a transition from asynchronous firing to population bursting could be induced by a reduction of I_K via a direct suppression of the potassium conductance or through an elevation of extracellular potassium concentration. Similar population bursting activity could be triggered by an augmentation of I_{NaP}. These findings are discussed in the context of the possible role of population bursting activity in the pBC in the respiratory rhythm generation in vivo vs. in vitro and during normal breathing in vivo vs. gasping.

1 Introduction

The pre-Bötzinger complex (pBC) is a small region in the rostroventrolateral medulla that is considered to be an essential part of the brainstem respiratory neural network (Gray et al. 2001; Rekling and Feldman 1998; Schwarzacher et al. 1995; Smith et al. 1991). As shown in vitro, this region can, under certain conditions, generate an intrinsic rhythmic bursting activity (Johnson et al. 1994; Koshiya and Smith 1999; Rekling and Feldman 1998; Smith et al. 1991; Thoby-Brisson and Ramirez 2001). This rhythmic activity remains after blockade of synaptic inhibition in vitro (Feldman and Smith 1989; Shao and Feldman 1997). Therefore, it has been suggested that this activity is driven by a subpopulation of pacemaker bursting neurons located within the pBC (Butera et al. 1999a, b; Del Negro et al. 2001; Rekling and Feldman 1998; Koshiya and Smith 1999; Smith 1997; Smith et al. 2000; Thoby-Brisson and Ramirez 2001).

Analysis of possible intrinsic cellular mechanisms for endogenous bursting activity in the pBC led to the suggestion that this activity is most likely generated with a necessary contribution of persistent sodium current (Butera et al. 1999a,b; for an opposing view see Del Negro et al. 2002b). Butera et al. (1999a) offered the first computational model of a pBC pacemaker neuron whose bursting was based on the persistent sodium current. This elegant computational model was then extended in subsequent computational studies by the same group (Butera et al. 1999b; Del Negro et al. 2001; Smith et al. 2000). The model reproduced a number of experimental phenomena and offered a series of experimental predictions. However, because the persistent sodium channels had not been experimentally characterized in pBC neurons at the time the model was developed, the authors used generic descriptions for the kinetics of ionic channels including those for the fast and persistent sodium channels.

We recently performed experimental characterization of both rapidly inactivating and persistent sodium currents in neurons from the rostroventrolateral medulla including the pBC (Rybak et al. 2003a; Shevtsova et al. 2002). The voltage-gated characteristics of both types of sodium currents obtained in these studies differed from those used in the models by Butera et al. (1999a,b) and Del Negro et al. (2001). Therefore, one objective of the present study was to evaluate the results of the previous modeling studies using formal descriptions of sodium channel kinetics drawn from our experiments.

The "hybrid pacemaker-network" theory of respiratory rhythmogenesis suggests that a subpopulation of pacemaker neurons in the pBC comprises a rhythm-generating "kernel" that drives a wider respiratory pattern-forming network (e.g., see Butera et al. 1999a,b;

Correspondence to: I. A. Rybak
(e-mail: rybak@cbis.ece.drexel.edu)

Rekling and Feldman 1998; Smith et al. 2000). The existence of a pacemaker-driven kernel can explain the resistance of the in vitro rhythm to blockade of inhibitory synaptic transmission (Ballanyi et al. 1999; Shao and Feldman 1997). Previous network theories and models of respiratory rhythm generation were critically based on the presence of reciprocal inhibition between different populations of respiratory neurons and hence failed to explain this phenomenon. At the same time, the earlier network models were able to reproduce and explain many systems-level phenomena, including the independent regulation of inspiratory and expiratory phases, respiratory reflexes, phase resettings and phase transitions produced by stimulation of afferent nerves, etc. (e.g., see Balis et al. 1994; Botros and Bruce 1990; Duffin 1991; Duffin et al. 1995; Gottschalk et al. 1994; Lindsey et al. 2000; Ogilvie et al. 1992; Rybak et al. 1997a,b). These are the systems-level phenomena that are very difficult to explain if the rhythm is exclusively controlled by a pacemaker-driven mechanism.

In this regard, several attempts have recently been made toward the development of a unified computational model that could maintain the advantages of both the above approaches and hence would be consistent with both in vivo and in vitro data. It has been proposed that, subject to the conditions, the respiratory rhythm can be generated by either a network or a hybrid mechanism (Rybak et al. 2001, 2002; Smith et al. 2000). This attractive idea immediately raises key questions: What are the operational conditions for each mechanism, and how can the system switch from one mechanism to another? An associated second objective of the present study was to investigate the possible roles of the persistent sodium and potassium currents in triggering or suppressing the endogenous bursting activity in the pBC.

According to the hybrid pacemaker-network model (Smith et al. 2000), the pacemaker-driven kernel located in the pBC is incorporated into a wider respiratory network and hence may receive inputs and feedback from other respiration-related areas. This is consistent with the demonstration of the existence of connectivity among neurons in different regions of the ventral medullary respiratory network (e.g., see Ellenberger and Feldman 1990; Morillo et al. 1995; Zheng et al. 1998). Excitatory and inhibitory rhythmic afferent inputs to the pacemaker bursting neurons in the pBC may interact with their endogenous rhythmogenic properties and hence modify firing behavior of these neurons. Therefore, the rhythmic bursting activity generated in the pBC may be dependent on a dynamic interplay between endogenous and forced oscillations. A computational investigation of such interactions was also an objective of the present study.

2 Methods

2.1 Single neuron model

Our model of the pBC pacemaker neuron is a typical single-compartment neuron model based on the Hodgkin-Huxley formal description. The model is a modified version of the earlier models developed by Butera et al. (1999a, Model 1) and Del Negro et al. (2001). The modeled neuron included the following ionic currents (and the corresponding ionic conductances): rapidly inactivating (or fast) sodium (I_{Naf} with the maximal conductance $\bar{g}_{Naf}$); persistent sodium (I_{NaP} with the maximal conductance $\bar{g}_{NaP}$); noninactivating delayed-rectifier potassium (I_K with the maximal conductance $\bar{g}_K$); leakage (I_{leak} with the conductance g_{leak}), and synaptic excitatory (I_{synE} with the conductance g_{synE}) and inhibitory (I_{synI} with the conductance g_{synI}) currents – which together defined the dynamics of the neuronal membrane potential V:

$$C \cdot \frac{\mathrm{d}V}{\mathrm{d}t} = -I_{Naf} - I_{NaP} - I_K - I_{leak} - I_{synE} - I_{synI} \ , \qquad (1)$$

where ionic currents are described as follows:

$$\begin{aligned} I_{Naf} &= \bar{g}_{Naf} \cdot m_{Naf}^3 \cdot h_{Naf} \cdot (V - E_{Na}), \\ I_{NaP} &= \bar{g}_{NaP} \cdot m_{NaP} \cdot h_{NaP} \cdot (V - E_{Na}), \\ I_K &= \bar{g}_K \cdot m_K^4 \cdot (V - E_K), \\ I_{leak} &= g_{leak} \cdot (V - E_{leak}), \\ I_{synE} &= g_{synE} \cdot (V - E_{synE}), \\ I_{synI} &= g_{synI} \cdot (V - E_{synI}) \ , \end{aligned} \qquad (2)$$

and C is the whole cell capacitance and t is time.

Activation m_i and inactivation h_i of the voltage-gated channel i (e.g., fast sodium, *Naf*, persistent sodium, *NaP*, or delayed-rectifier potassium, *K*) are described by the following differential equations:

$$\begin{aligned} \tau_{mi}(V) \cdot \frac{\mathrm{d}}{\mathrm{d}t} m_i &= m_{\infty i}(V) - m_i \ , \\ \tau_{hi}(V) \cdot \frac{\mathrm{d}}{\mathrm{d}t} h_i &= h_{\infty i}(V) - h_i \ , \end{aligned} \qquad (3)$$

where the steady-state voltage-dependent activation and inactivation are described by Boltzmann functions as follows:

$$\begin{aligned} m_{\infty i}(V) &= (1 + \exp(-(V - V_{1/2mi})/k_{mi}))^{-1} \ , \\ h_{\infty i}(V) &= (1 + \exp((V - V_{1/2hi})/k_{hi}))^{-1} \ . \end{aligned} \qquad (4)$$

The voltage-dependent time constants for activation and inactivation are described in the following form (Butera et al. 1999a):

$$\begin{aligned} \tau_{mi}(V) &= \frac{\bar{\tau}_{mi}}{\cosh((V - V_{1/2mi})/k_{\tau mi})} \ , \\ \tau_{hi}(V) &= \frac{\bar{\tau}_{hi}}{\cosh((V - V_{1/2hi})/k_{\tau hi})} \ . \end{aligned} \qquad (5)$$

In (4) and (5), $V_{1/2mi}$ and $V_{1/2hi}$ are, respectively, half activation and half inactivation voltages for channel i, k_{mi} and k_{hi} are the corresponding slope factors of activation and inactivation, $\bar{\tau}_{mi}$ and $\bar{\tau}_{hi}$ are the maximal time constants of activation and inactivation, respectively, and $k_{\tau mi}$ and $k_{\tau hi}$ are the corresponding slope factors for activation and inactivation time constants.

The reversal potentials for sodium (E_{Na}) and potassium (E_K) channels are defined by the Nernst equation

$$E_i = \frac{R \cdot T}{z_i \cdot F} \cdot \ln \frac{[X_i]_o}{[X_i]_{in}} \quad , \tag{6}$$

where R is the universal gas constant, T is the temperature in Kelvin degrees, F is Faraday's constant, $[X_i]_o$ is the concentration of ions i outside the cell, and $[X_i]_{in}$ is the concentration of these ions inside the cell. The reversal potential for leakage channels is modeled using the Goldman equation

$$E_{leak} = \frac{R \cdot T}{Z_i \cdot F} \ln \frac{[K^+]_o + P_{Na/k}[Na^+]_o}{[K^+]_{in} + P_{Na/k}[Na^+]_{in}} \quad , \tag{7}$$

where $p_{Na/K}$ is the relative permeability of Na^+ ions (with respect to permeability of K^+ ions) at rest.

The reversal potentials for excitatory (E_{synE}) and inhibitory (E_{synI}) synaptic channels were considered constant. The conductances of these channels (g_{synE} and g_{synI}) were equal to zero at rest. Each of these conductances had two components: one defining external drive to the neuron (excitatory g_{Edr} or inhibitory g_{Idr}, respectively) and the other defining inputs from other neurons in the network (g_{Enet} or g_{Inet}, respectively):

$$\begin{aligned} g_{synE} &= g_{Edr} + g_{Enet} \quad , \\ g_{synI} &= g_{Idr} + g_{Inet} \quad . \end{aligned} \tag{8}$$

For single neuron simulations, $g_{Enet} = g_{Inet} = 0$, and g_{Edr} and g_{Idr} were used as variables defining external excitatory and inhibitory synaptic inputs to the neuron.

2.2 Population model

In this study, only excitatory interconnections within neural populations were considered ($g_{Inet} = 0$). The excitatory synaptic interactions between the neurons were simulated in the following way. At rest, $g_{Enet} = 0$. Each spike arriving from a neuron j to the excitatory synapse of neuron i increased the synaptic conductance by $\bar{g}_E \cdot w_{ji}$, where w_{ji} is the synaptic weight of the excitatory input from neuron j to neuron i and $\bar{g}_E$ is the parameter defining an increase in the synaptic conductance produced by one spike at $w_{ji} = 1$. The dynamics of synaptic conductance in neuron i produced by the excitatory synaptic inputs was described as follows:

$$g_{Eneti}(t) = \bar{g}_E \cdot \sum_{j(j \neq i)} w_{ji} \cdot \sum_{t_{kj} < t} \exp(-(t - t_{kj})/\tau_{synE}) \quad , \tag{9}$$

where τ_{synE} defines the synaptic time constant and t_{kj} defines the time of the effect of the k-th spike from a neuron j on the synaptic conductance of neuron i (in our model, t_{kj} corresponds to a moment when the falling edge of incoming action potential reaches the level of -10 mV, which emulates a "synaptic delay" approximately equal to the duration of action potential, i.e., about 1 ms).

In all simulations described in this report, we considered neural populations consisting of $N = 50$ neurons fully interconnected with excitatory synaptic connections.

2.3 Selection of model parameters

Parameters used in our simulations are shown in Table 1. In some cases, when the values of parameters differed from those in Table 1, the used values are noted in the text or corresponding figure legend.

All voltage-gated and kinetic parameters for the fast sodium channels as well as the maximal conductance and voltage-gated parameters for the persistent sodium channel activation were explicitly drawn from our experimental studies (Rybak et al. 2003a; Shevtsova et al. 2002).

Several experimental studies have demonstrated that persistent sodium channels slowly inactivate (Baker and Bostock 1998; Fleidervish et al. 1996; Fleidervish and Gutnick 1996; Magistretti and Alonso 1999; etc.). However, this slow inactivation has not been well characterized. The parameters of inactivation for persistent sodium current, namely, the half inactivation voltage for the persistent sodium channel ($V_{1/2hNaP} = -57.0$ mV), the slope factor for inactivation ($k_{hNaP} = 3.0$ mV), and the maximal inactivation time constant ($\bar{\tau}_{\tau hNaP} = 20000$ ms) and the time constant slope factor ($k_{\tau hNaP} = 6.0$ mV) were chosen during preliminary simulations to produce an experimentally observed burst frequencies and durations. The half inactivation voltage in our model was within the range of the reported values (e.g., -56.2 mV in Baker and Bostock 1998; -52.6 mV in Magistretti and Alonso 1999), whereas the value for the maximal inactivation time constant was larger than that estimated experimentally (e.g., Magistretti and Alonso (1999) reported that $\bar{\tau}_{\tau hNaP} = 6000$ to 6500 ms; Butera et al. (1999a) used $\bar{\tau}_{\tau hNaP} = 10000$ ms). Due to a lack of experimental data, the maximal time constant for activation of persistent sodium current was assumed equal to that of the fast sodium current ($\bar{\tau}_{mNaP} = \bar{\tau}_{mNaf}$). The slope factors for the time constants of persistent sodium channel activation and inactivation were set at twice the value of the slope factors for the voltage-dependent activation and inactivation, respectively: $k_{\tau mNaP} = 2 \cdot k_{mNaP}$ and $k_{\tau hNaP} = 2 \cdot k_{hNaP}$; see expressions (2)–(4) and subsequent explanations in Butera et al. (1999a).

Delayed-rectifier potassium channels have not been experimentally characterized in the pBC and other respiration-related areas. We modified and used the voltage-gated characteristics for activation of this channel from the model of thalamocortical neurons by McCormick and Huguenard (1992). This model was taken as a basis because the voltage-gated characteristics of the fast sodium current drawn from our experimental studies were the closest to those in the model of McCormick and Huguenard. The delayed-rectifier potassium and fast sodium currents together define the cellular spike-generation mechanism, and the stability of this mechanism requires certain relationships between the characteristics of voltage-dependent activation of these currents. We assumed

Table 1. Model parameters

Ionic channel parameters	
Fast sodium:	
activation	$V_{1/2mNaf} = -43.8$ mV; $k_{mNaf} = 6.0$ mV; $\bar{\tau}_{mNaf} = 0.9$ ms; $k_{\tau mNaf} = 14.0$ mV
inactivation	$V_{1/2hNaf} = -67.5$ mV; $k_{hNaf} = 10.8$ mV; $\bar{\tau}_{\tau hNaf} = 35.2$ ms; $k_{\tau hNaf} = 12.8$ mV
maximal conductance	$\bar{g}_{Naf} = 150$ nS
Persistent sodium:	
activation	$V_{1/2mNaP} = -47.1$ mV; $k_{mNaP} = 3.1$ mV; $\bar{\tau}_{mNaP} = 0.9$ ms; $k_{\tau mNaP} = 6.2$ mV
inactivation	$V_{1/2hNaP} = -57.0$ mV; $k_{hNaP} = 3.0$ mV; $\bar{\tau}_{\tau hNaP} = 20{,}000$ ms; $k_{\tau hNaP} = 6.0$ mV
maximal conductance	$\bar{g}_{NaP} = 4.0$ nS (basic value)
Delayed-rectifier potassium:	
activation	$V_{1/2mK} = -44.5$ mV; $k_{mK} = 5.0$ mV; $\bar{\tau}_{mK} = 4.0$ ms; $k_{\tau mK} = 10.0$ mV
maximal conductance	$\bar{g}_K = 50.0$ nS (basic value)
Leakage	$g_{leak} = 2.0$ nS (basic value)
Neuron parameters	
Ionic concentrations and reversal potentials	$[Na^+]_{in} = 15$ mM, $[Na^+]_o = 145$ mM ($E_{Na} = 60$ mV at $T = 308$ K) $[K^+]_{in} = 140$ mM, $[K^+]_o = 4$ mM (basic value), ($E_K = -94$ mV at $[K^+]_o = 4$ mM) $p_{Na/K} = 0.03$ ($E_{leak} = -76$ mV at $[K^+]_o = 4$ mM) $E_{synE} = 0$ mV, $E_{synI} = -80$ mV
Membrane capacitance	$C = 36.2$ pF
Network/population parameters	
Synaptic connections	$\bar{g}_E = 0.1$ nS; $\tau_{synE} = 5$ ms
Random distribution of parameters in the population	$\bar{g}_{NaP} = 4.0 \pm 0.4$ nS; $\bar{g}_K = 50.0 \pm 5.0$ nS; $g_{leak} = 2.0 \pm 0.2$ nS; $g_{Edr} = 0.12 \pm 0.012$ nS; $w_{ij} = 0.2 \pm 0.02$ N = 50
Constants and other parameters	
	$R = 8.3143 \cdot 10^3$ J/(KM·K); $F = 9.648 \cdot 10^4$ C/M; $T = 308$ K

that the relationships between voltage-dependent activation of fast sodium and delayed-rectifier potassium channels in the rat pBC neurons are the same as those in the rat thalamocortical neurons. To apply this assumption, the curve of voltage-dependent activation for delayed-rectifier potassium current from the model of McCormick and Huguenard (1992) was shifted to more negative values of voltage and its slope was modified in such a way that the voltage-dependent activation of the delayed-rectifier potassium current in our model was in the same voltage relationship (in the half activation voltage and activation threshold) with the fast sodium activation curve as in the original model of McCormick and Huguenard (1992). The resultant curve of voltage-dependent activation of the delayed-rectifier potassium channel was then fitted to a fourth-degree Boltzmann function (see (2) and (4)) to define the half activation voltage and slope factor for this channel ($V_{1/2mK} = -44.5$ mV; $k_{mK} = 5.0$ mV). The maximal activation time constant and slope factor were set as follows: $\bar{\tau}_{mK} = 4.0$ ms; $k_{\tau mK} = 2 \cdot k_{mK}$. The basic value of the maximal conductance of this channel was set to $\bar{g}_K = 50.0$ nS, which was found to be optimal for stable spike and burst generation.

Intracellular and extracellular concentrations of sodium and potassium ions and the relative permeability of Na^+ ions with respect to permeability of K^+ ions (see Table 1) were set to meet average data for neurons in the mammalian nervous system (Johnson and We 1997). The reversal potentials for sodium and potassium currents were calculated on the basis of the Nernst equation (6). The leakage reversal potential was calculated using the Goldman equation (7). The synaptic reversal potentials were: $E_{synE} = 0$ mV and $E_{synI} = -80$ mV. The value of the whole cell capacitance, $C = 36.2$ pF, was based on experimental measurements of membrane capacitance in neurons dissociated from the rostroventrolateral medulla of rat (Kawai et al. 1999). The leakage conductance, $g_{leak} = 2$ nS, was set to fit the experimentally measured minimal cell input resistance $R_{in} = 500$ MΩ (Mazza et al. 2000). The values of membrane capacitance ($C = 36.2$ pF) and input resistance ($R_{in} = 500$ MΩ) were consistent with the corresponding values measured by Del Negro et al. (2002a) in pBC neurons: $C = 32 \pm 3$ pF and $R_{in} = 430 \pm 56$ MΩ for identified pacemaker neurons.

To investigate the dependence of firing characteristics (spike or burst frequency, burst duration, etc.) or the dependence of neuronal firing behavior (such as "silence", "bursting", or "tonic activity") on various model parameters, we ran series of stimulations while changing each selected parameter with a particular step and represented the obtained results in the form of regular one-dimensional plots or 2D diagrams of parameters. In these simulations, the following step sizes were generally used: 0.1 mM for $[K^+]_o$, 0.01 nS for g_{Edr}, 0.1 nS for $\bar{g}_{NaP}$, and 2 nS for $\bar{g}_K$. In the vicinity of the dramatic changes in neuronal firing behavior observed, steps reduced ten times were used for a more accurate determination of the measured firing characteristics or the positions of borders between the parameter regions corresponding to different types of firing behavior. In all these cases, the values of firing parameters measured or the type of firing behavior were estimated during a stationary mode, i.e., after all transitional processes following a stepwise change of each model parameter had been completed.

In all simulations of neural populations, some key parameters of neurons within the populations were randomly distributed over neurons in these populations.

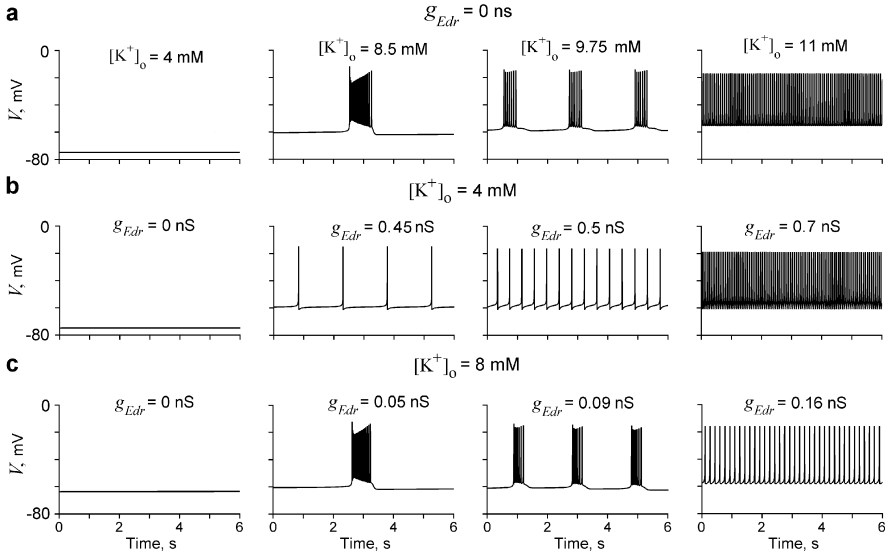

Fig. 1. Firing activity of model of single pacemaker neuron under different conditions. **a** Firing behavior of model without excitatory drive ($g_{Edr} = 0$) at different levels of extracellular potassium concentration ($[K^+]_o$). $[K^+]_o$ increases from *left* to *right*. An increase in $[K^+]_o$ triggers the rhythmic bursting activity at some threshold of $[K^+]_o$. Further increase in $[K^+]_o$ produces an increase in burst frequency and decrease of burst duration. At a higher level of $[K^+]_o$, bursting switches to tonic firing. **b** Firing behavior of model at $[K^+]_o = 4$ mM. g_{Edr} increases from *left* to *right*. An increase in g_{Edr} causes an increase in the frequency of tonic activity. **c** Firing behavior of model at $[K^+]_o = 8$ mM. g_{Edr} increases from *left* to *right*. Bursting activity is triggered when g_{Edr} exceeds some threshold. The frequency of bursts increases with an increase in g_{Edr} until the neuron switches to tonic firing at a higher level of g_{Edr}

Specifically, to incorporate heterogeneity in neurons within a population, the maximal conductances of persistent sodium ($\bar{g}_{NaP}$), delayed-rectifier potassium ($\bar{g}_K$) and leakage (g_{leak}) channels in particular neurons, as well as external drives to these neurons (g_{Edr}) and weight of synaptic inputs (w_{ij}) were randomly assigned from a normal distribution using average values and variances of these parameters (see Table 1).

2.4 Computer simulation

All simulations were performed on a Pentium IV computer, 1.7 GHz/512 MB (DELL) with MS Windows 2000 operating system using a special simulation package *NSM 1.0* developed at Drexel University by I.A. Rybak, S.N. Markin, D.G. Ivashko, and N.A. Shevtsova. Differential equations were solved using the exponential Euler integration method (McGregor 1987) with the integration step of 0.1 ms. To test the accuracy of the numerical solutions of differential equations by this method at the integration step used, the single neuron simulations were also run using a variable order integration method (ode15s) available in *MATLAB* 6.0 (MathWorks, Inc.) The differences between the simulation results obtained by using the above two methods were less than 10^{-4} for each variable.

3 Results

3.1 Endogenous bursting activity in single pacemaker neurons: the roles of tonic excitatory drive and extracellular potassium concentration

The developed model of a single pBC pacemaker neuron demonstrated the ability to generate rhythmic bursting activity under certain conditions (within a particular region of the parameter space). Figure 1a shows that an increase in extracellular potassium concentration ($[K^+]_o$) triggered rhythmic bursting activity at some $[K^+]_o$ threshold. As $[K^+]_o$ increased further, burst frequency increased with a concomitant decrease in burst duration. At a higher level of $[K^+]_o$, bursting activity switched to tonic firing. In contrast, an increase in the tonic excitatory drive to the neuron (g_{Edr}) at a normal level of $[K^+]_o$ (4 mM) did not produce bursting but increased frequency of tonic activity (Fig. 1b). At a higher level of $[K^+]_o$ (e.g., at $[K^+]_o = 8$ mM; see Fig. 1c), bursting activity was triggered when g_{Edr} exceeded some threshold. The frequency of bursts increased with an increase in g_{Edr} until the neuron switched to tonic firing at a higher level of g_{Edr} (Fig. 1c).

As described in detail by Butera et al. (1999a), the burst generation mechanism in this model is explicitly dependent on the slow voltage-dependent inactivation of the persistent sodium current (h_{NaP}), which increases slowly during interburst periods and decreases during burst periods (Fig. 2a). Comparison of the amplitudes of the persistent sodium (I_{NaP}) and the delayed-rectifier (I_K) currents during spikes showed that both the amplitude of I_{NaP} and the ratio of the amplitudes I_{NaP}/I_K were much higher in the bursting mode than during tonic activity (compare Fig. 2a and b).

To investigate the dependence of neuronal firing behavior on model parameters, we ran series of simulations while changing the values of $[K^+]_o, g_{Edr}$ and maximal conductances of persistent sodium, delayed-rectifier potassium, and leak channels. The results of these simulations are shown in Figs. 3 and 4.

Figure 3a–c (middle column) shows regions corresponding to different modes of single cell activity as a

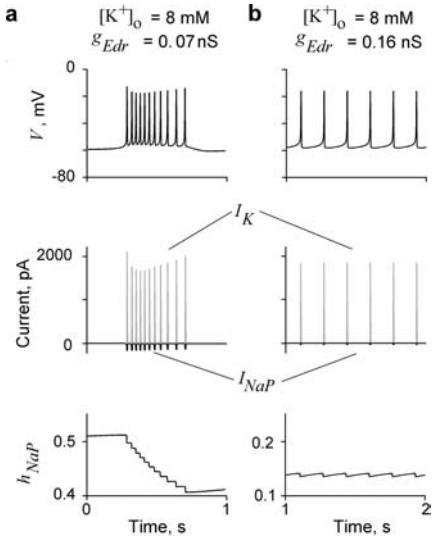

Fig. 2. Dynamics of the neuronal membrane potential (V, *top trace*), the persistent sodium (I_{NaP}, *middle trace*, *black line*) and delayed-rectifier (I_K, *middle trace*, *gray line*) potassium currents, and the persistent sodium inactivation variable h_{NaP} (*bottom trace*) during bursting (**a**) and tonic (**b**) activity, respectively

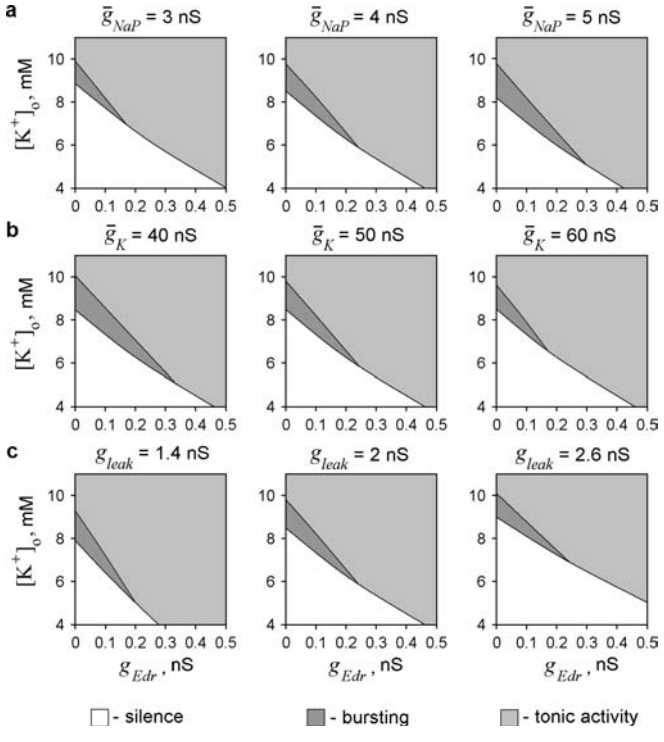

Fig. 3. Regions for "silence", "bursting", and "tonic activity" modes in single-cell firing behavior as a function of g_{Edr} and $[K^+]_o$. The middle column corresponds to the basic values of model parameters ($\bar{g}_{NaP}$ = 4.0 nS; $\bar{g}_K$ = 50.0 nS; g_{leak} = 2.0 nS). **a–c** Shifting the borderlines between the regions caused by changes in maximal conductances of the persistent sodium $\bar{g}_{NaP}$ (**a**), delayed-rectifier $\bar{g}_K$ (**b**), and leakage g_{leak} (**c**) channels, respectively. The maximal conductances increase from *left* to *right*

function of g_{Edr} and $[K^+]_o$ at the basic values of model parameters ($\bar{g}_{NaP} = 4.0$ nS; $\bar{g}_K = 50.0$ nS; $g_{leak} = 2.0$ nS). It is seen that bursting behavior occurs only

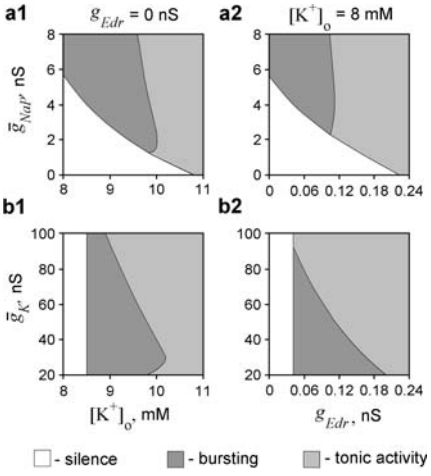

Fig. 4. Regions for "silence", "bursting", and "tonic activity" as a function of $\bar{g}_{NaP}$ and $[K^+]_o$ (**a1** and **a2**), and as a function of $\bar{g}_K$ and $[K^+]_o$ (**b1** and **b2**). In **a1** and **b1**, $g_{Edr} = 0$. In **a2** and **b2**, $[K^+]_o = 8$ mM

within a small region of the parameter space (g_{Edr} and $[K^+]_o$). At $g_{Edr} = 0$, the bursting region is the widest: bursting occurs from $[K^+]_o = 8.5$ to 9.8 mM (or within the range of values of the potassium reversal potential E_K from −74.4 to −70.6 mV).

3.2 Balance and interplay between the persistent sodium, delayed-rectifier potassium, and leakage currents

Our simulations have demonstrated that the firing behavior of the model depends on the relationships between the three major currents I_{NaP}, I_K, and I_{leak}. The critical role of the relationship between the persistent sodium (I_{NaP}) and voltage-independent leakage (I_{leak}) currents for the neuronal ability to generate intrinsic bursting activity was previously suggested (Del Negro et al. 2001, 2002a). In contrast, the role of the voltage-gated potassium currents (e.g., the delayed-rectifier) and their relationships with I_{NaP} and I_{leak} in the generation of endogenous bursting have not been investigated.

In each diagram in Fig. 3, three separate regions in $([K^+]_o, g_{Edr})$ coordinate space represent the three different modes of single neuron firing behavior: "silence", "bursting", and "tonic activity". These regions are separated by two borderlines, one of which defines the threshold of neuronal firing ("threshold borderline"), and the other separates regions for bursting and tonic activities ("bursting borderline"). Figure 3a–c shows shifts of these borderlines resulting from changes in the maximal conductances of the persistent sodium ($\bar{g}_{NaP}$), delayed-rectifier potassium ($\bar{g}_K$), and leakage (g_{leak}) channels, respectively.

The position of the threshold borderline is mostly controlled by $\bar{g}_{NaP}$ and g_{leak}, (Fig. 3a,c) and is almost independent of $\bar{g}_K$ (Fig. 3b). An increase in $\bar{g}_{NaP}$ or a decrease of g_{leak} shifts this borderline to lower values of g_{Edr} and $[K^+]_o$ and hence widens the bursting region. A decrease of $\bar{g}_{NaP}$ or an increase in g_{leak} produces the

opposite effect. Hence, according to our results, the relationship between I_{NaP} and I_{leak} actually defines not the ability of the cell to generate endogenous bursts (as suggested by Del Negro et al. 2001, 2002a), but rather the cellular excitability in general. This relationship controls switching between the bursting and silence states only at lower values of excitatory drive and higher values of $[K^+]_o$ (Fig. 3a,c).

The position of the bursting borderline is mostly controlled by $\bar{g}_K$ and g_{leak} (Fig. 3b,c), and is almost independent of $\bar{g}_{NaP}$ (Fig. 3a). An increase in $\bar{g}_K$ or a decrease of g_{leak} shifts this borderline to lower values of g_{Edr} and $[K^+]_o$ and constricts the bursting region. A decrease of $\bar{g}_K$ or an increase in g_{leak} produces the opposite effect. Hence, switching between the bursting and tonic modes in single neuron firing behavior is mostly controlled by I_K and its relation with I_{leak}, but not by I_{NaP}.

Importantly, I_{leak} almost does not influence the size of the bursting region. Instead, a reduction of I_{leak} shifts this region to lower values of excitatory drive and $[K^+]_o$ (Fig. 3c). In contrast, changes of I_{NaP} and I_K produce opposite effects on the size of the bursting region (Fig. 3a,b) and hence their balance or imbalance is important for inducing endogenous bursting.

Another important conclusion from the analysis of each diagram in Fig. 3 is that an increase in excitatory drive to the neuron and an increase in $[K^+]_o$ produce different effects on neuronal firing behavior. Specifically, an increase in g_{Edr} at a normal level of $[K^+]_o$ depolarizes the cell without changing the balance between I_{NaP} and I_K. A relatively large I_K provides a strong membrane repolarization after each generated spike. This strong repolarization lowers the membrane potential below the level of I_{NaP} activation and hence prohibits endogenous bursting.

In contrast, an increase in $[K^+]_o$ produces two simultaneous effects: one is cellular depolarization via shifting the leakage reversal potential E_{leak} to more positive values of voltage; see (7); and the other is suppression of I_K by shifting the potassium reversal potential E_K to more positive values of voltage; see (6) and (2). Therefore, at higher levels of $[K^+]_o$, the reduced I_K does not produce the sufficient afterspike repolarization and hence cannot restrain endogenous I_{NaP}-dependent bursting activity.

3.3 Triggering endogenous bursting activity in single pacemaker neurons

Figure 4 represents regions for "silence", "bursting", and "tonic activity" described above as functions of $\bar{g}_{NaP}$ and $[K^+]_o$, $\bar{g}_{NaP}$ and g_{Edr}, $\bar{g}_K$ and $[K^+]_o$, and $\bar{g}_K$ and g_{Edr}. These diagrams, together with the diagrams in Fig. 3, predicted that endogenous bursting in single neuron could be triggered from the silence mode either by the elevation of $[K^+]_o$ (Fig. 4a1,b1 and Fig. 3) or by the appropriate augmentation of $\bar{g}_{NaP}$ (Fig. 4a1,a2). At the same time, a transition from a tonic activity to bursting might occur following a suppression of $\bar{g}_K$ (Fig. 4b1,b2).

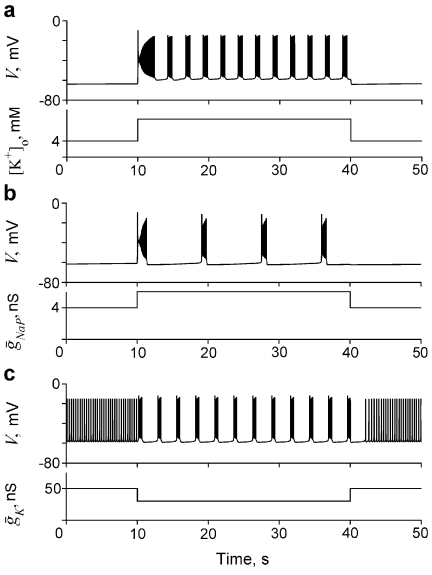

Fig. 5. Triggering endogenous bursting activity in the model of single pBC pacemaker neuron: **a** by an elevation of the extracellular potassium concentration ($[K^+]_o$, *bottom trace*) and **b** by an augmentation of the maximal conductance of the persistent sodium channel ($\bar{g}_{NaP}$, *bottom trace*). **c** Transition from tonic activity to bursting following a reduction in the maximal conductance of potassium channel ($\bar{g}_K$, *bottom trace*)

The above predictions were explicitly tested in our simulations (see Fig. 5). In Fig. 5a, endogenous bursting in the neuron was triggered by an elevation of the extracellular potassium concentration $[K^+]_o$. In Fig. 5b, the neuron was switched to bursting by an increase in the maximal conductance of the persistent sodium channels $\bar{g}_{NaP}$. In Fig. 5c, the transition from tonic activity to bursting was produced by a reduction of the maximal conductance of the delayed-rectified potassium channels $\bar{g}_K$.

3.4 Frequency and duration of endogenous bursts generated by a single pacemaker neuron

The dependence of burst frequency and burst duration on various model parameters and excitatory drive were studied with two major objectives: to examine the theoretical conclusions of previous simulation performed by Butera et al. (1999a) and Del Negro et al. (2001) and to study the dependences of burst frequency and burst duration on $\bar{g}_K$, which were not considered in the previous models. Figure 6 summarizes our results in these modeling studies.

In Fig. 6, all plots were drawn for the bursting regions of parameters. We limited our investigation to two cases. In the first case, we fixed $g_{Edr} = 0$ and induced bursting by elevating $[K^+]_o$ (Fig. 6a1, a3, b1, b3, c1, c3), and in the second case we fixed $[K^+]_o = 8$ mM and induced bursting by increasing g_{Edr} (Fig. 6a2, a4, b2, b4, c2, c4). The first case approximately corresponded to the previous modeling studies by Del Negro et al. (2001, Fig. 2C–F), whereas the second case was similar to

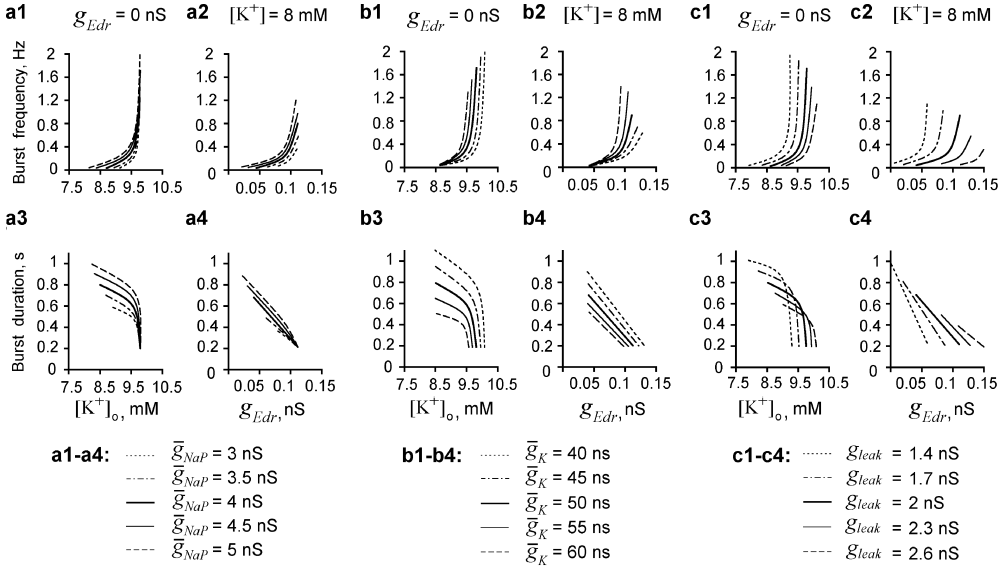

Fig. 6. Dependences of the burst frequency (**a1**, **a2**; **b1**, **b2**; **c1**, **c2**) and burst duration (**a3**, **a4**; **b3**, **b4**; **c3**, **c4**) upon extracellular potassium concentration $[K^+]_o$ (**a1**, **a3**; **b1**, **b3**; **c1**, **c3;** in all plots $g_{Edr} = 0$) and excitatory drive g_{Edr} (**a2**, **a4**; **b2**, **b4**; **c2**, **c4;** in all plots $[K^+]_o = 8$ mM) at different values of maximal conductances of ionic channels ($\bar{g}_{NaP}$, $\bar{g}_K$, g_{leak}). The *thick solid line* in each plot corresponds to the basic set of model parameters

the previous simulations of Butera et al. (1999a, Fig. 6 B1,B3).

Each curve in Fig. 6 was produced by changing the variable depicted in the *x*-axis with a fixed step and calculating the burst frequency and duration. The set of curves in each plot shows variation of burst frequency and duration resulting from changes in the maximal conductances of the persistent sodium ($\bar{g}_{NaP}$), delayed-rectifier potassium ($\bar{g}_K$), and leakage (g_{leak}) channels. At the basic set of model parameters, the burst frequency increased with an increase in $[K^+]_o$, and the increase in frequency became almost exponential when $[K^+]_o$ approached the borderline between the regions for bursting and tonic activity (Fig. 6a1–c1, solid lines). The duration of bursts decreased with an increase in $[K^+]_o$, and this decrease became abrupt by the edge of the bursting region (Fig. 6a3–c3). These changes of burst frequency and duration were similar to those described earlier by Del Negro et al. (2001, Fig. 2C–F) and consistent with the experimental data (Del Negro et al. 2001, Fig. 4C,D; Koshiya and Smith 1999). The increase in burst frequency with the increase in g_{Edr} was similar to that during elevation of $[K^+]_o$ but did not normally exceed 1.0–1.2 Hz (Fig. 6a2–c2). The corresponding decrease of burst duration was almost linear within the bursting region (Fig. 6a4–c4). These changes of burst frequency and duration were similar to those described earlier by Butera et al. (1999a, Fig. 6B1,B3).

Augmentation of $\bar{g}_{NaP}$ produced an increase in both burst frequency and burst duration (Fig. 6a1–a4) similar to that in the models by Butera et al. (1999a) and Del Negro et al. (2001). Augmentation of $\bar{g}_K$ also produced an increase in frequency but reduced burst duration (Fig. 6b1–b4). An increase in g_{leak} significantly shifted the region of bursting. It also decreased burst frequency, similar to that in the model of Del Negro et al. (2001), and produced a nonuniform effect on burst duration (Fig. 6c1–c4).

3.5 Modeling a population of pacemaker neurons with excitatory connections

To investigate the firing behavior of a population of pacemaker neurons, we modeled a population of 50 neurons with all-to-all excitatory synaptic connections. To incorporate heterogeneity in neurons within the population, some intrinsic parameters of the neurons ($\bar{g}_{NaP}$, $\bar{g}_K$ and g_{leak}), external drive (g_{Edr}), and weights of neuronal interconnections (w_{ij}) were assigned from normal distributions (Table 1).

Our simulations have shown that both the excitatory synaptic interactions between neurons and the randomization of neuronal parameters within the population make the region of parameters for population bursting wider than that for a single pacemaker neuron (see also Butera et al. 1999b and Del Negro et al. 2001).

Figure 7 shows an example of our simulations. An increase in $[K^+]_o$ to exceed some threshold (7.9±0.4 mM) triggered bursting activity in the population (Fig. 7a). Further increase in $[K^+]_o$ produced an increase in burst frequency and a desynchronization of neuronal activities, which in turn caused a decrease in burst amplitude and an increase in the level of asynchronous activity. At a higher level of $[K^+]_o$, the population bursting activity switched to a high-level asynchronous firing (Fig. 7a).

An increase in g_{Edr} at the basic level of $[K^+]_o$ (4 mM) did not produce bursting in the population but increased the level of asynchronous activity (Fig. 7b). At higher values of $[K^+]_o$ (e.g., at $[K^+]_o = 6$ mM, see Fig. 7c), population bursting was triggered when g_{Edr} exceeded some threshold (0.19 ± 0.04 nS). The frequency of bursts increased with an increase in g_{Edr}. However, increasing g_{Edr} produced a desynchronization of neuronal activities, which in turn decreased the amplitude of population bursts and increased the level of asynchronous activity. Finally, at some level of g_{Edr}, firing behavior of the population switched to a high-level asynchronous firing (Fig. 7c).

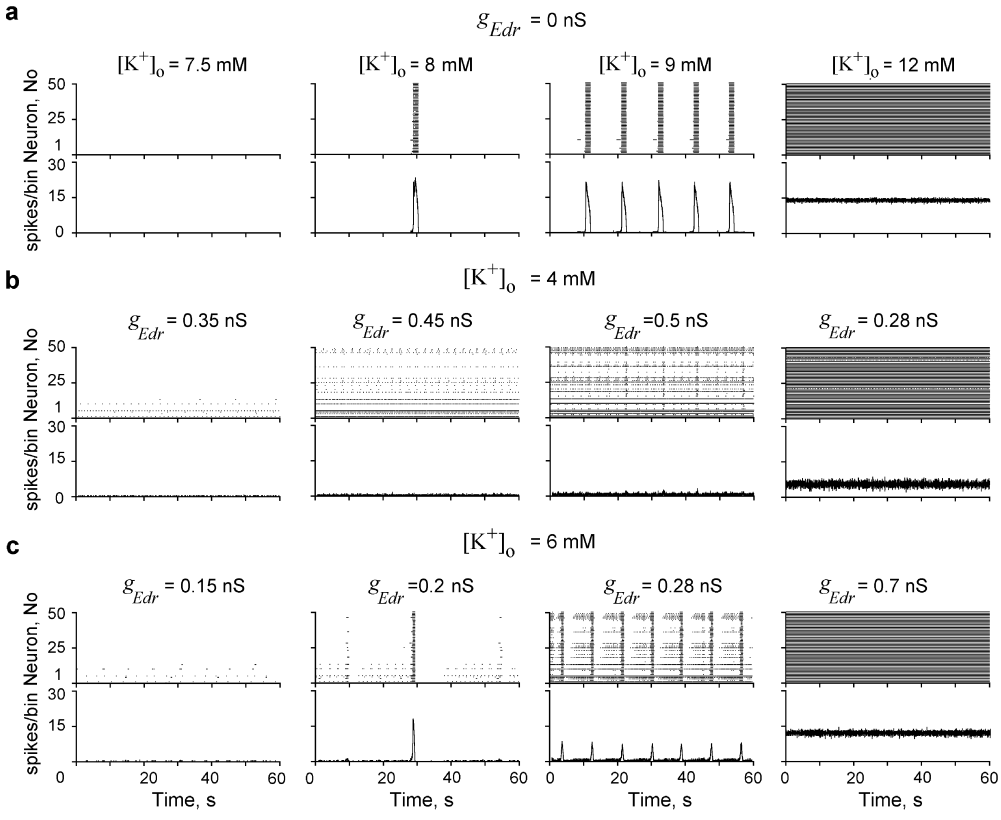

Fig. 7. Firing activity of a model of population of pacemaker neurons under different conditions. The result of each simulation is represented by two diagrams: the *top diagram* is a raster plot for spike times in all 50 cells, sorted on the ordinate axis by cell index number; the *bottom diagram* is a corresponding integrated histogram of population activity (bin size = 10 ms). **a** Example of firing behavior of the model without excitatory drive ($g_{Edr} = 0$) at different levels of $[K^+]_o$. $[K^+]_o$ increases from *left* to *right*. **b** Example of firing behavior of the model at $[K^+]_o$ = 4 mM and different levels of excitatory drive g_{Edr}. **c** Example of firing behavior of the model at $[K^+]_o$ = 6 mM and different levels of g_{Edr}. In **b** and **c**, the mean value of g_{Edr} in the population increases from *left* to *right*

Firing bursts generated in the population could be generally classified by shape into two types (Fig. 8a,b). One type of burst resulted from a synchronization of endogenous bursts of individual neurons and had a typical high-amplitude decrementing shape (Fig. 8a). The population bursting activity of this type was generated at relatively high concentrations of $[K^+]_o$ and low level of g_{Edr}. The high concentration of $[K^+]_o$ sufficiently reduced I_K in a large group of neurons to switch them to the bursting mode. Therefore, even weak excitatory interactions could synchronize bursts of individual neurons and form this type of population bursting.

Bursts of the second type (''group-pacemaker-like'') were formed with the essential contribution of the excitatory synaptic interactions between the neurons. This burst type started with a slight ramp and had a relatively low amplitude (Fig. 8b). In this case, most individual neurons involved in the formation of population bursts did not generate the ''typical endogenous bursts'' (having a fast onset followed by a decrementing spiking frequency). Interestingly, these neuronal bursts were similar to those of the Type-I pBC pacemaker neuron described by Gray et al. (1999) and/or to the neuronal bursts of the ''slow bursters'' described by Thoby-Brisson and Ramirez (2001). Importantly, this type of population bursting usually occurred at a relatively low concentration of $[K^+]_o$ but required certain levels of both g_{Edr} and mutual excitatory interactions.

Increasing randomization of individual neuron parameters (e.g., an increase in the variances of $\bar{g}_{NaP}$, $\bar{g}_K$, and g_{leak}) could induce multiple (usually double) bursting activities synchronized with frequency ratio from 1:2 to 1:10 (see an example in Fig. 9). This double-bursting firing behavior in the model was very similar to so-called ''fictive eupnoea'' and ''sighs'' generated simultaneously in the pBC under certain conditions in vitro as described by Thoby-Brisson and Ramirez (2001).

The formal description of the mechanism and conditions for generation and coexistence of the above different types of population bursting activity requires special mathematical investigation and is beyond the scope of this paper. A qualitative explanation of this mechanism is the following. An increased randomization of neuronal parameters resulted in the formation (within the population) of neuronal ''clusters'' with different but overlapping bursting regions in the parameter space. Depending on the parameter values $([K^+]_o, g_{Edr}, w_{ij})$, each cluster could ''take over'' and force the other neurons and other clusters to oscillate with its ''own'' frequency. At the same time, when the parameter values corresponded to the overlapping bursting zone, oscillations with different frequencies could coexist and be stable. The ''low-frequency cluster'' synchronized a larger number of neurons (including neurons from the ''high-frequency cluster'') and hence had larger amplitude of population bursting (Fig. 9).

3.6 Triggering bursting activity in the model of neural population

Similar to triggering endogenous bursting activity in a single pacemaker neuron, a synchronized population

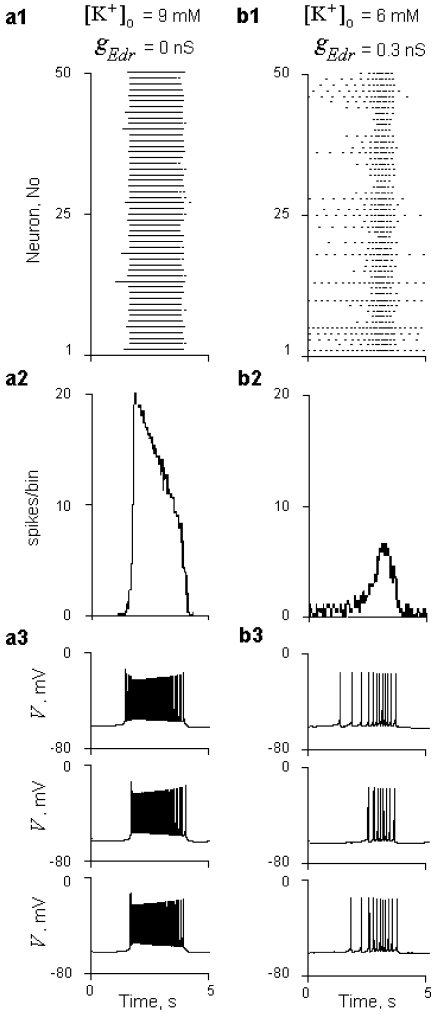

Fig. 8. Representative examples of two types of population bursts (**a1**–**a3** and **b1**–**b3**, respectively). **a1** and **b1** show the corresponding raster plots; **a2** and **b2** show integrated histograms of population activity; **a3** and **b3** demonstrate examples of activities of individual neurons

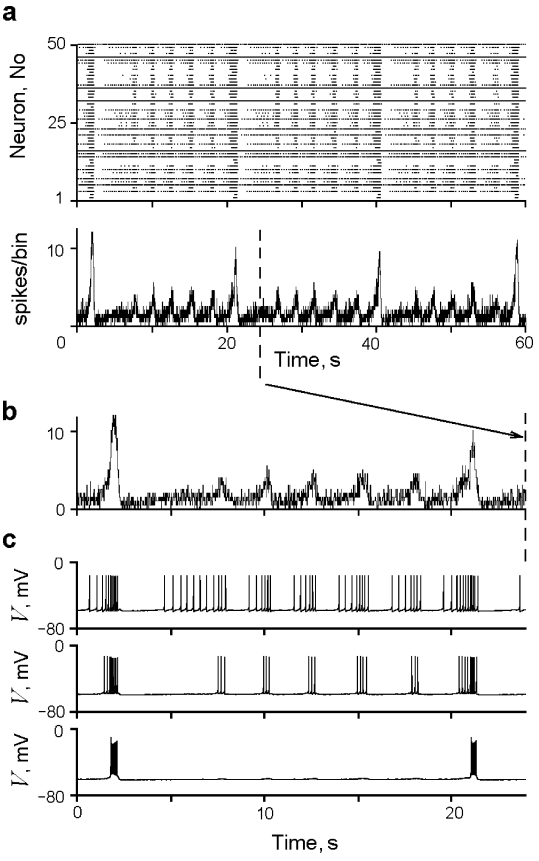

Fig. 9. Representative example of double-bursting activity in the population model. **a** Raster plot and integrated histogram of population activity. **b** Integrated histogram at expanded time scale. **c** Examples of activities of individual neurons. Simulation was performed at $[K^+]_o$ = 5.7 mM and $g_{Edr} = 0.3$ nS

bursting activity in the model could be initiated by either an elevation of $[K^+]_o$ or an alteration in $\bar{g}_K$ or $\bar{g}_{NaP}$ in the population. However, the region of the parameter space producing bursting was significantly wider for the population than for single pacemaker neurons. The necessary elevation of $[K^+]_o$ ($[K^+]_o$ threshold) for triggering population bursting activity decreased with an increase in the excitatory drive to the population. Figure 10a shows an example in which population bursting activity was triggered by the increase in $[K^+]_o$ from the basic level (4 mM) to 7.2 mM at $g_{Edr} = 0.15$ nS.

Population bursting activity could be triggered at the basic level of $[K^+]_o$ by either an augmentation of $\bar{g}_{NaP}$ (Fig. 10b) or a reduction of $\bar{g}_K$ (Fig. 10c) in all neurons of the population. In the former example (Fig. 10b), the $\bar{g}_{NaP}$ augmentation induced multiple bursting activity similar to that in Fig. 9.

3.7 Frequency and amplitude of population bursts in the population model

The population model was used to study the dependence of frequency and amplitude of population bursts generated in the bursting mode on several model parameters. The results of these studies are shown in Fig. 11. The dependence of frequency and amplitude of population bursts on $[K^+]_o$ were studied in the absence of external excitatory drive ($g_{Edr} = 0$, see Fig. 11a1,a2). Burst frequency increased monotonically with the elevation of $[K^+]_o$ within the bursting region (Fig. 11a1). The burst amplitude slightly increased initially (because of the increasing number of intrinsically bursting neurons) and then dramatically decreased with the elevation of $[K^+]_o$ because of desynchronization of individual neuron activities (Fig. 11a2). The dependences of frequency and amplitude of population bursts on the excitatory drive g_{Edr} (at $[K^+]_o = 8$ mM) were qualitatively similar to their dependencies on $[K^+]_o$ (Fig. 11b1,b2). The burst frequency also increased with an increase in either $\bar{g}_{NaP}$ (Fig. 11c1) or $\bar{g}_K$ (Fig. 11d1). An increase in $\bar{g}_{NaP}$ initially caused an augmentation in the burst amplitude, because of the increasing number of

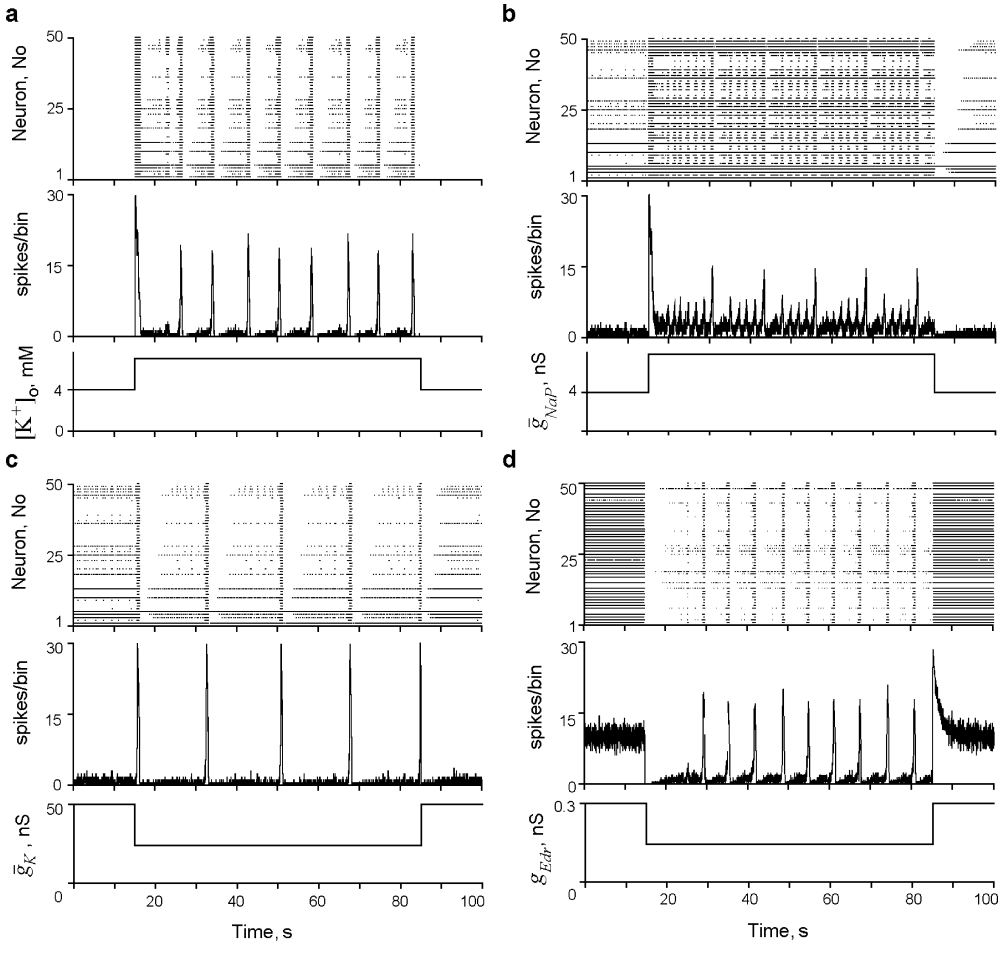

Fig. 10. Triggering endogenous bursting activity in the population model. **a** Triggering endogenous bursting by an elevation of $[K^+]_o$ (*bottom trace*). $[K^+]_o$ increased from 4 to 7.2 mM at $g_{Edr} = 0.15$ nS. **b** Triggering endogenous bursting by an augmentation of the mean value of $\bar{g}_{NaP}$ (*bottom trace*). The mean value of $\bar{g}_{NaP}$ increased from 4 to 8 nS at $[K^+]_o = 4$ mM and $g_{Edr} = 0.47$ nS. **c** Triggering endogenous bursting by a reduction of the mean value of $\bar{g}_K$ in the population (*bottom trace*). The mean value of $\bar{g}_K$ was reduced from 50 to 25 nS at $[K^+]_o$ = 4 mM and $g_{Edr} = 0.47$ nS. **d** Transition from asynchronous activity to population bursting by a reduction of g_{Edr} (*bottom trace*). The mean value of g_{Edr} was reduced from 0.3 to 0.15 nS. at $[K^+]_o = 7.2$ mM

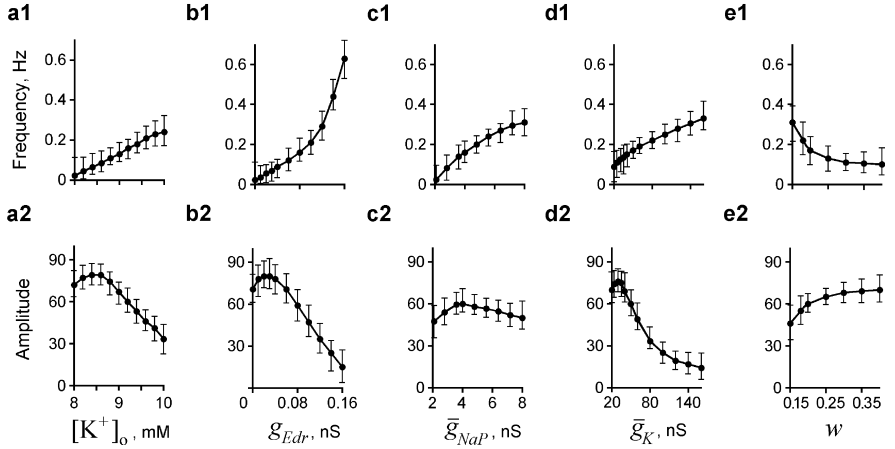

Fig. 11. The dependence of frequency (**a1**–**e1**) and amplitude (**a2**–**e2**) of population bursts upon various model parameters: $[K^+]_o$ (at $g_{Edr} = 0$; **a1**, **a2**); g_{Edr} (at $[K^+]_o = 8$ mM; **b1**, **b2**); $\bar{g}_{NaP}$ (at $[K^+]_o = 8$ mM and $g_{Edr} = 0.08$ nS; **c1**, **c2**); $\bar{g}_K$ (at $[K^+]_o = 8$ mM and $g_{Edr} = 0.08$ nS; **d1**, **d2**); w (at $[K^+]_o = 8$ mM and $g_{Edr} = 0.08$ nS; **e1**, **e2**). Each diagram represents average values ± SD and was developed based on ten simulations with reinitialization of neuronal parameters. In **c1**, **c2**, **d1**, **d2**, **e1**, and **e2**, the varied parameter ($\bar{g}_{NaP}$, $\bar{g}_K$, or w, respectively) was not randomized and was set the same in all neurons of the population

intrinsically bursting neurons, and then a decrease of the amplitude, because more and more neurons were transformed to tonic firing (Fig. 11c2). An increase in $\bar{g}_K$ produced a dramatic decrease in the burst amplitude because of the reduction in the number of intrinsically bursting neurons (Fig. 11d2). Similar to the model of Butera et al. (1999b), an increase in the weights of the excitatory synaptic interconnections within the population reduced burst frequency (Fig. 11e1) and increased burst amplitude (Fig. 11e2). The latter occurred because the increasing w_{ij} increased neuronal synchronization. The former occurred since the pacemakers with lower intrinsic frequencies were able to synchronize the population.

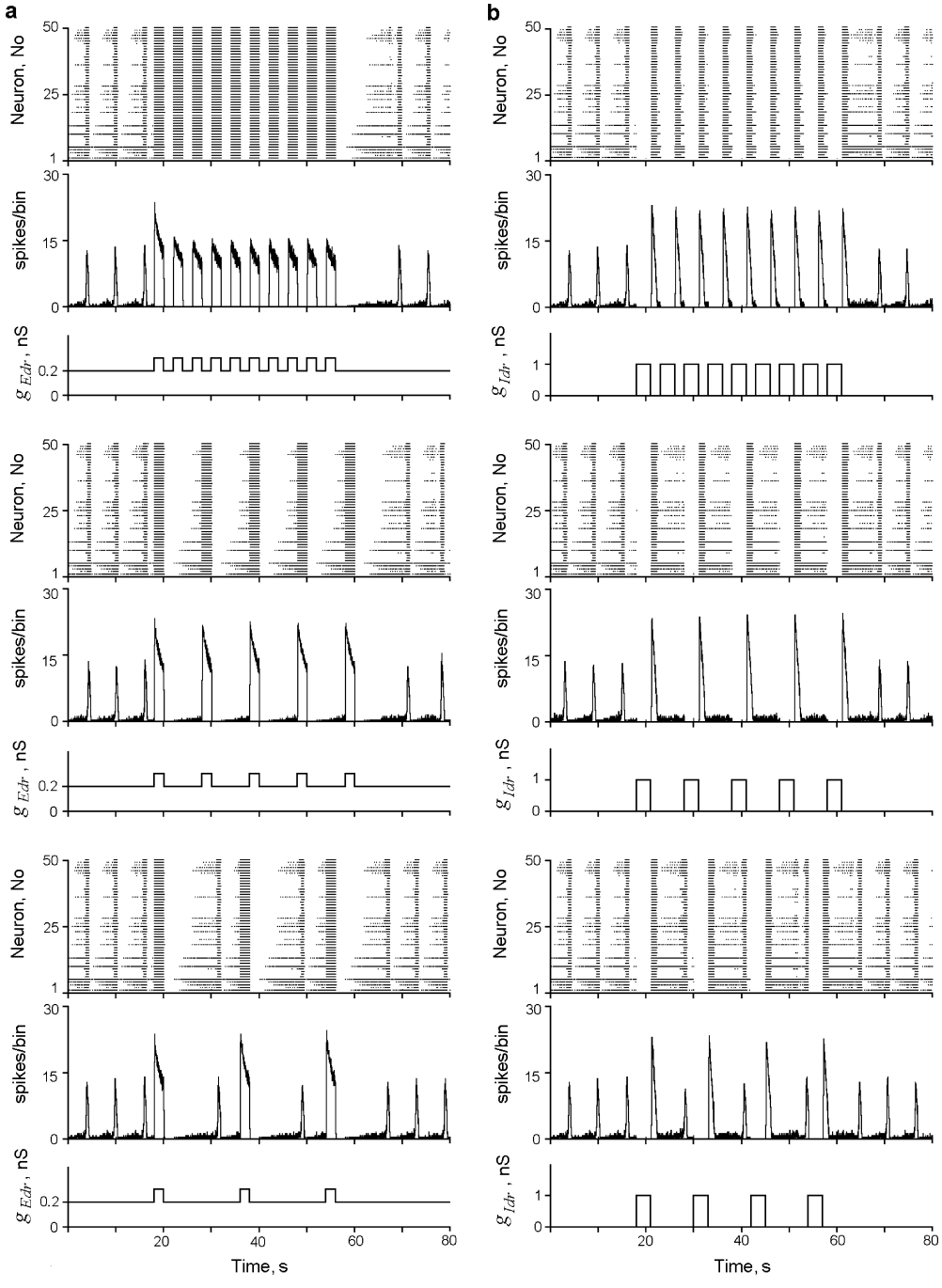

Fig. 12. Examples of responses of the population model to the application of excitatory (**a**) and inhibitory (**b**) rhythmic stimulation. In all cases the external rhythmic drive (*bottom traces*) was applied to the population operating in the mode of endogenous bursting activity ($[K^+]_o$ = 7 mM and $g_{Edr} = 0.2$ nS). The frequency of stimulating pulses decreases from *top* to *bottom*

3.8 Response of the model to rhythmic stimulation: interaction between endogenous and forced rhythmic bursting activities

To study possible interactions between the endogenous rhythmogenic mechanism and external rhythmic drives, we applied rhythmic excitatory or inhibitory drives to all neurons of the population operating in the population bursting mode. Figure 12a,b shows representative examples of these computational experiments. The excitatory rhythmic drive was added to the tonic drive (Fig. 12a). Application of excitatory pulses whose frequency was higher (top diagram) or up to 1.5 times lower (middle diagram) than the frequency of endogenous bursts forced the generation of population bursting activity with frequency and timing of bursts explicitly defined by the external stimulation. A lower frequency of stimulation allowed for the appearance of endogenous bursts in addition to the forced bursts (bottom diagram).

Each external inhibitory pulse produced a rebound population burst (Fig. 12b). The rhythmic inhibitory stimulation with a frequency higher (top diagram) or up to 1.5 times lower (middle diagram) than the frequency of endogenous bursts induced a forced

population bursting activity in which frequency and timing of the bursts were defined by the external rhythmic inhibitory drive. A lower frequency of stimulation permitted the generation of endogenous bursts in addition to the forced bursts (bottom diagram).

4 Discussion

4.1 Evaluation of the persistent-sodium-based model of pBC pacemaker neurons

The basic persistent-sodium-based model of single pacemaker neurons and populations of these neurons were developed by Butera et al. (1999a,b) and elaborated by Del Negro et al. (2001) with the objective of simulating and explaining the generation of pacemaker-driven neural oscillations in the pBC in vitro. As was mentioned in the introduction, these models were based on generic descriptions of sodium ionic channels. The voltage-gated characteristics of both fast and persistent sodium channels drawn from our experimental studies in neurons acutely dissociated from the pBC area differed from those used in the models of Butera et al. (1999a,b) and Del Negro et al. (2001). However, despite differences in model parameters, our modeling studies confirmed most of the previous results and conclusions by Butera et al. (1999a,b) and Del Negro et al. (2001). Specifically, we have demonstrated the general ability of the model to generate population bursting with the shapes of single neuron discharges and population bursts similar to those recorded from the pBC in vitro (see, e.g., Figs. 1 and 7). We confirmed the possibility of triggering the population bursting activity by the elevation of extracellular potassium concentration (see Figs. 7 and 10). In addition, we determined the functional dependence of the burst characteristics (frequency and duration of neuronal bursts, frequency and amplitude of population bursts) on the $[K^+]_o$, cellular excitability (g_{Edr}), and other parameters (e.g., weights of excitatory synaptic interconnections) at both the single neuron (Fig. 6) and population (Fig. 11) levels. Therefore, our modeling results provide additional support for the theoretical concept that a voltage-dependent persistent-sodium-based mechanism (initially described by Butera et al. (1999a,b)) can mediate population bursting activity in the pBC in vitro.

An attempt to experimentally reevaluate the role of the persistent-sodium-based mechanism for the generation of bursting activity in the pBC in vitro was recently made by Del Negro et al. (2002b). The authors found that rhythmic activities in the medullary slice preparation continued following a pharmacological blockade of persistent sodium channels by riluzole. However, this finding appears to be at variance with the reports from several laboratories in which riluzole could block the endogenous rhythmic activity in pBC in vitro (Koizumi and Smith 2002; Parkis et al. 2002; Pierrefiche et al. 2002; Rybak et al. 2003b). Del Negro et al. (2002b) did not test neurons located deep in slices. It is tempting to speculate that a reason for this discrepancy is the poor penetration of riluzole into the tissue in the experiments by Del Negro et al. (2002b). However, these authors clearly demonstrated the blockade of persistent sodium current in all of the neurons they examined. At the same time, the doses used (up to 200 μM) were large enough to also block rapidly inactivating sodium current as shown in dissociated neurons (Herbert et al. 1994; Song et al. 1997; K. Ptak, G. Zummo, G.F. Alheid, D.J. Surmeier, D.R. McCrimmon, unpublished observations). Therefore, the roles of pacemaker- and network-based mechanisms in the pBC rhythmic activity in vitro require further experimental investigations.

Similar to the models by Butera et al. (1999b) and Del Negro et al. (2001), our model was able to generate I_{NaP}-dependent endogenous bursts. These high-amplitude bursts with a decrementing shape were similar to those recorded from the phrenic nerve during gasping. Recent in vivo studies in the cat have demonstrated that the pBC may serve in vivo as "a central hypoxia chemosensor" whose activation by sodium cyanide elicits a "rapid series of high-amplitude, rapid rate of rise, short-duration inspiratory bursts that are indistinguishable from gasps produced by severe systemic hypoxia" (Solomon et al. 2000; Solomon 2002). Importantly, sodium cyanide is known to produce two effects: a focal hypoxia-like state in the pBC (Kawai et al. 1999; Mazza et al. 2000) and an additional activation of I_{NaP} (Hammarström and Gage 2000; Kawai et al. 1999). In addition, the generation of I_{NaP}-dependent bursting activity in both our and Butera et al. (1999b) models does not require inhibition. This is consistent with the data that rhythmic activity recorded in vitro remains after blockade of synaptic inhibition (Feldman and Smith 1989; Shao and Feldman 1997). As recently shown, gasping also appears to be resistant to blockade of inhibition (St.-John and Paton 2002; St.-John et al. 2002). Therefore, it is possible that both our and Butera et al. models actually describe a I_{NaP}-dependent pacemaker-driven mechanism in the pBC playing a key role in the generation of gasping.

4.2 The role of voltage-gated potassium currents and interplay between I_{NaP} and I_K

Our modeling studies have demonstrated that firing behavior of both single pacemaker neurons and populations of these neurons essentially depends on specific complex relationships between the persistent sodium and delayed-rectifier potassium currents. Specifically, a release or suppression of the I_{NaP}-dependent pacemaker bursting mechanism depends on (and may be controlled by) the level of expression of potassium currents. The normally expressed I_K provides a strong membrane repolarization after each generated spike. It hyperpolarizes the membrane below the level of I_{NaP} activation and hence prohibits endogenous bursting. Consequently, endogenous bursting in the population can be triggered by either a suppression of I_K (e.g., through a reduction of $\bar{g}_K$; Fig. 10c) or an augmentation of I_{NaP} (e.g., via an increase in $\bar{g}_{NaP}$; Fig. 10b).

In most studies using in vitro preparations, robust endogenous bursting activity in the pBC was produced and maintained by the elevation of the extracellular potassium concentration up to 7–9 mM (e.g., see Koshiya and Smith 1999; Lieske et al. 2000; Shao and Feldman 1997; Thoby-Brisson and Ramirez 2001), although less reliable bursting could be produced at low levels of $[K^+]_o$, for example, after pharmacological blockade of inhibition (Johnson et al. 1994). The major conclusion from our modeling studies is that the endogenous bursting activity in the pBC can be induced by an imbalance between the persistent sodium and voltage-gated potassium currents. Specifically, triggering endogenous bursting in the pBC by the elevation of $[K^+]_o$, the method commonly used in most in vitro preparations, can occur because of the reduction of potassium currents caused by the elevation of $[K^+]_o$.

An important question is how an increase in $[K^+]_o$ triggers endogenous bursting in the pBC. The effect of an elevation of $[K^+]_o$ on cellular behavior differs from a simple increase in cellular excitability. Indeed, an increase in $[K^+]_o$ should produce a cellular depolarization by shifting the leakage reversal potential to more positive values of voltage. In addition, however, the elevation of $[K^+]_o$ reduces all voltage-gated potassium currents by shifting the potassium reversal potential to more positive voltage values. As a result, at higher levels of $[K^+]_o$, the reduced voltage-gated potassium currents cannot restrain the endogenous I_{NaP}-dependent bursting activity.

The important role of voltage-gated potassium currents in the generation of endogenous bursting activity in the pBC in vitro has recently been experimentally demonstrated by Pierrefiche et al. (2002) and Rybak et al. (2003b), who reported that rhythmic bursting in the same medullary slice could be triggered by either an application of potassium current blockers (TEA or 4-AP) at $[K^+]_o = 3$ mM or an elevation of $[K^+]_o$ to 5–7 mM.

4.3 Endogenous bursting in the pBC and generation of the respiratory rhythm

The ability of the pBC to generate endogenous rhythmic bursting activity has been demonstrated in vitro in many studies. However, the relation of the rhythm recorded in vitro to the normal (''eupnoeic'') respiratory rhythm generated in vivo or other forms of breathing, such as gasping, is still a subject of intense debate.

As indicated above, recent in vivo studies have suggested that the pBC may serve as a central hypoxia chemosensor (Solomon et al. 2000; Solomon 2002). Previous experimental studies revealed that hypoxia causes (i) an increase in the external potassium concentration $[K^+]_o$ (Melton et al. 1996), (ii) a suppression of voltage-gated potassium currents (Conforti and Millhorn 1997; Gebhardt and Heinemann 1999; Jiang and Haddad 1994; Liu et al. 1999; Lopez-Barneo et al. 2001; Thompson and Nurse 1998), and (iii) an augmentation of the persistent sodium current (Hammarström and Gage 1998, 2000, 2002; Horn and Waldrop 2000; Kawai et al. 1999). In the present study, we investigated the effects of the above three factors accompanying hypoxia on the firing behavior of the model of a population of pacemaker neurons in the pBC. We have shown that each of these factors, namely, an increase in $[K^+]_o$ (Fig. 10a), a reduction of $\bar{g}_K$ (Fig. 10b), and an augmentation of $\bar{g}_{NaP}$ (Fig. 10c), can trigger the pacemaker-driven population rhythm. Hence our present computational results support the idea that gasping in vivo may be driven by a pacemaker mechanism originating in the pBC.

4.4 Possible interaction between the network-based and pacemaker-driven rhythmogenic mechanisms

The network theories of the respiratory rhythm generation suggest that the respiratory rhythm in vivo derives from inhibitory network interactions between functionally different neural populations (e.g., see von Euler 1986; Feldman 1986; Richter 1996). According to the hybrid pacemaker-network concept, the pacemaker-driven kernel located in the pBC is incorporated into a broader respiratory network (Smith et al. 2000) and hence may receive inputs and feedback from other respiration-related areas. Moreover, the latest version of the hybrid pacemaker-network model also suggests that the respiratory rhythm may be generated in a mode in which ''none of the kernel neurons exhibit intrinsic pacemaker-like oscillations'' (Smith et al. 2000). This is consistent with the idea of the coexistence of two different rhythmogenic mechanisms. Specifically, Fukuda (2000) suggests that one of these mechanisms, a ''secondary'' or a ''gasping type'', corresponds to a (pacemaker-driven) generator found in vitro. If two such rhythmogenic mechanisms do coexist with a dominant role of the ''primary'' generator of a network type, then what is the possible behavior of the ''secondary'' generator during generation of the eupnoeic rhythm? Our computational study has demonstrated that both excitatory (Fig. 12a) and inhibitory (Fig. 12b) rhythmic inputs to the population of pacemaker neurons (with pulse frequencies within the range of breathing frequency in mammals) may force this population to produce a rhythmic bursting output whose frequency is explicitly defined by the input rhythmic drive. This allows the suggestion that, under normal in vivo conditions in which inhibitory interactions are strongly expressed, the network rhythmogenic mechanism operating in the entire respiratory network (including the pBC as an important part of the network) may overcome the pacemaker-driven rhythmogenic mechanisms operating within the pBC. Alternatively, during hypoxic gasping when inhibition is suppressed (Richter et al. 1991; Schmidt et al. 1995), a pacemaker-driven mechanism in the pBC may release, become dominant, and drive oscillations in the entire respiratory network (see also Rybak et al. 2000, 2002; St.-John et al. 2002).

Acknowledgements. This work was supported by NSF (0091942), NIH (NS046062-2) and ONR (N000140210086) grants to Ilya A. Rybak and NIH grants (HL60097, HL60969 and HL072415-01) to Donald R. McCrimmon.

References

Baker MD, Bostock H (1998) Inactivation of macroscopic late Na^+ current and characteristics of unitary late currents in sensory neurons. J Neurophysiol 80: 2538–2549

Balis UJ, Morris KF, Koleski, J, Lindsey, BG (1994) Simulations of a ventrolateral medullary neural network for respiratory rhythmogenesis inferred spike train cross-correlation. Biol Cybern 70: 311–327

Ballanyi K, Onimaru H, Homma I (1999) Respiratory network function in the isolated brainstem-spinal cord of newborn rat. Prog Neurobiol 59: 583–634

Botros SM, Bruce EN (1990) Neural network implementation of the three-phase model of respiratory rhythm generation. Biol Cybern 63: 143–153

Butera RJ, Rinzel JR, Smith JC (1999a) Models of respiratory rhythm generation in the pre-Bötzinger complex. I: Bursting pacemaker neurons. J Neurophysiol 82: 382–397

Butera RJ, Rinzel JR, Smith JC (1999b) Models of respiratory rhythm generation in the pre-Bötzinger complex. II: Populations of coupled pacemaker neurons. J Neurophysiol 82: 398–415

Conforti L, Millhorn DE (1997) Selective inhibition of a slow-inactivating voltage-dependent K + channels in rat PC12 cells by hypoxia. J Physiol Lond 502: 293–305

Duffin J (1991) A model of respiratory rhythm generation. Neuroreport 2: 623–626

Duffin, J, Ezure K, Lipski J (1995) Breathing rhythm generation: focus on rostral ventrolateral medulla. News Physiol Sci 10: 133–140

Del Negro CA, Johnson SM, Butera RJ, Smith JC (2001) Models of respiratory rhythm generation in the pre-Bötzinger complex. III: Experimental tests of model predictions. J Neurophysiol 86: 59–74

Del Negro CA, Koshiya N, Butera RJ, Smith JC (2002a) Persistent sodium current, membrane properties and bursting behaviour of pre-Bötzinger complex inspiratory neurons in vitro. J Neurophysiol 88: 2242–2250

Del Negro CA, Morgado-Valle C, Feldman JL (2002b) Respiratory rhythm: an emergent network property? Neuron 34: 821–830

Ellenberger HH, Feldman JL (1990) Brainstem connections of the rostral ventral respiratory group of the rat. Brain Res 513: 35–42

Feldman JL (1986) Neurophysiology of breathing in mammals. In: Bloom FE (ed) Handbook of physiology, sect 1, vol 4. American Physiology Society, Bethesda, MD, pp 463–524

Feldman JL, Smith JC (1989) Cellular mechanisms underlying modulation of breathing pattern in mammals. Ann NY Acad Sci 563: 114–130

Fleidervish IA, Friedman A, Gutnick MJ (1996) Slow inactivation of Na+ current and slow cumulative spike adaptation in mouse and guinea-pig neocortical neurones in slices. J Physiol 493(1): 83–97

Fleidervish IA, Gutnick MJ (1996) Kinetics of slow inactivation of persistent sodium current in layer V neurons of mouse neocortical slices. J Neurophysiol 76: 2125–2130

Fukuda Y (2000) Respiratory neural activity responses to chemical stimuli in newborn rats: reversible transition from normal to 'secondary' rhythm during asphyxia and its implication for 'respiratory like' activity in isolated medullary preparation. Neurosci Res 38: 407–417

Gebhardt C, Heinemann U (1999) Anoxic decrease in potassium outward currents of hippocampal cultured neurons in absence and presence of dithionite. Brain Res 837: 270–276

Gray PA, Janczewski WA, Mellen N, McCrimmon DR, Feldman JA (2001) Normal breathing requires pre-Bötzinger complex neurokinin-1 receptor-expressing neurons. Nat Neurosci 4: 927–930

Gray PA, Rekling JC, Bocchiaro CM, Feldman JL (1999) Modulation of respiratory frequency by peptidergic input to rhythmogenic neurons in the pre-Bötzinger complex. Science 286: 1566–1568

Gottschalk A, Ogilvie MD, Richter DW, Pack AI (1994) Computational aspects of the respiratory pattern generator. Neural Comput 6: 56–68

Hammarström AK, Gage PW (1998) Inhibition of oxidative metabolism increases persistent sodium current in rat CA1 hippocampal neurons. J Physiol Lond 510: 735–741

Hammarström AK, Gage PW (2000) Oxygen-sensing persistent sodium channels in rat hippocampus. J Physiol Lond 529(1): 107–118

Hammarström AK, Gage PW (2002) Hypoxia and persistent sodium current. Eur Biophys J 31: 323–330

Hebert T, Drapeau P, Pradier L, Dunn RJ (1994) Block of the rat brain IIA sodium channel α-subunit by the neuroprotective drug riluzole. Mol Pharmacol 45: 1055–1060

Horn EM, Waldrop TG (1994) Hypoxic augmentation of fast-inactivating and persistent sodium currents in rat caudal hypothalamic neurons. J Neurophysiol 84: 2572–2581

Jiang C, Haddad GG (1994) A direct mechanism for sensing low oxygen levels by central neurons. Proc Natl Acad Sci USA 91: 7198–7201

Johnson SM, Smith JC, Funk GD, Feldman JL (1994) Pacemaker behaviour of respiratory neurons in medullary slices from neonatal rat. J Neurophysiol 72: 2598–2608

Johnson D, We M-S (1997) Foundations of Cellular Neurophysiology. MIT Press, Cambridge

Kawai Y, Qi J, Comer AH, Gibbons H, Win J, Lipski J (1999) Effects of cyanide and hypoxia on membrane currents in neurons acutely dissociated from the rostral ventrolateral medulla of the rat. Brain Res 830: 246–257

Koizumi H, Smith JC (2002) Perturbation of respiratory pattern and rhythm in vitro by block of persistent sodium current (INaP). Soc Neurosci Abstr 32: 173.6

Koshiya N, Smith JC (1999) Neuronal pacemaker for breathing visualized in vitro. Nature 400: 360–363

Lieske SP, Thoby-Brisson M, Telgkamp P, Ramirez JM (2000) Reconfiguration of the neural network controlling multiple breathing patterns: eupnoea, sighs and gasps. Nat Neurosci 3: 600–607

Lindsey BG, Morris KF, Segers LS, Shannon R (2000) Respiratory neuronal assemblies. Respir Physiol volume: 183–196

Liu H, Moczydlowski E, Haddad GG (1999) O_2 deprivation inhibits Ca^{2+}-activated K^+ channels via cytosolic factors in mice neocortical neurons. J Clin Invest 104: 577–588

Lopez-Barneo J, Pardal R, Ortega-Saenz P (2001) Cellular mechanisms of oxygen sensing. Annu Rev Physiol 63: 259–287

MacGregor RI (1987) Neural and brain modelling. Academic, New York

Magistretti J, Alonso A (1999) Biophysical properties and slow voltage-dependent inactivation of a sustained sodium current in entorhinal cortex layer-II principal neurons: a whole-cell and single-channel study. J Gen Physiol 114: 491–509

Mazza E Jr, Edelman NH, Neubauer JA (2000) Hypoxic excitation in neurons cultured from the rostral ventrolateral medulla of the neonatal rat. J Appl Physiol 88: 2319–2329

McCormick DA, Huguenard JR (1992) A model of the electrophysiological properties of thalamocortical relay neurons. J Neurophysiol 68: 1384–1400

Melton JE, Kadia SC, Yu QP, Neubauer JA, Edelman NH (1996) Respiratory and sympathetic activity during recovery from hypoxic depression and gasping in cats. J Appl Physiol 80: 1940–1948

Morillo AM, Nunez-Abades PA, Gaytan SP, Pasaro R (1995) Brain stem projections by axonal collaterals to the rostral and caudal ventral respiratory group in the rat. Brain Res Bull 37: 205–11

Ogilvie MD, Gottschalk A, Anders K, Richter DW, Pack AI (1992) A network model of respiratory rhythmogenesis. Am J Physiol (Reg) 263: R962–R975

Parkis MA, Pena F, Ramirez JM (2002) The role of pacemaker neurons in the generation of different respiratory rhythms. Soc Neurosci Abstr 32: 362.5

Pierrefiche O, Rybak IA, St-John WM, Paton, JFR (2002) Neurogenesis of respiratory rhythm: effects of suppression of potassium currents and hypoxia. Soc Neurosci Abstr 32: 173.11

Rekling JC, Feldman JL (1998) Pre-Bötzinger complex and pacemaker neurons: hypothesized site and kernel for respiratory rhythm generation. Annu Rev Physiol 60: 385–405

Richter DW (1996) Neural regulation of respiration: rhythmogenesis and afferent control. In: Greger R, Windhorst U (eds) Comprehensive human physiology, vol II. Springer, Berlin Heidelberg New York, pp 2079–2095

Rybak IA, Paton JFR, Schwaber JS (1997a) Modelling neural mechanisms for genesis of respiratory rhythm and pattern. II: Network models of the central respiratory pattern generator. J Neurophysiol 77: 2007–2026

Rybak IA, Paton JFR, Schwaber JS (1997b) Modelling neural mechanisms for genesis of respiratory rhythm and pattern. III: Comparison of model performances during afferent nerve stimulation. J Neurophysiol 77: 2027–2039

Rybak IA, St-John WM, Paton JFR (2001) Models of neuronal bursting behaviour: implications for in vivo versus in vitro respiratory rhythmogenesis. In: Poon CS, Kazemi H (eds) Frontiers in modelling and control of breathing: integration at molecular, cellular and systems levels. Plenum/Kluwer, New York, pp 159–164

Rybak IA, Paton, JFR, Rogers RF, St-John WM (2002) Generation of the respiratory rhythm: state-dependency and switching. Neurocomputing 44–46: 605–614

Rybak IA, Ptak K, Shevtsova NA, McCrimmon DR (2003a) Sodium currents in neurons from the rostroventrolateral medulla of the rat. J Neurophysiol 90: 1635–1642

Rybak IA, Shevtsova NA, St-John WM, Paton JFR, Pierrefiche O (2003b) Endogenous rhythm generation in the pre-Bötzinger complex and ionic currents: modelling and in vitro studies. Eur J Neurosci 18: 239–257

Schwarzacher S, Smith JC, Richter DW (1995) The pre-Bötzinger complex in the cat. J Neurophysiol 73: 1452–1461

Shao XM, Feldman JL (1997) Respiratory rhythm generation and synaptic inhibition of expiratory neurons in pre-Bötzinger complex: differential roles of glycinergic and gabaergic neural transmission. J Neurophysiol 77: 1853–1860

Shevtsova NA, Ptak K, McCrimmon DR, Rybak IA (2002) Study of sodium currents in neurons of pre-Bötzinger Complex. Soc Neurosci Abstr 32: 173.5

Smith JC (1997) Integration of cellular and network mechanisms in mammalian oscillatory motor circuits: insights from the respiratory oscillator. In: Stein PSG, Grillner S, Selverston AI, Stuart DG (eds) Neurons, networks, and motor behaviour. MIT Press, Cambridge, pp 97–104

Smith JC, Ellenberger HH, Ballanyi K, Richter DW, Feldman JL (1991) Pre-Bötzinger complex: a brainstem region that may generate respiratory rhythm in mammals. Science 254: 726–729

Smith JC, Butera RJ, Koshiya N, Del Negro C, Wilson CG, Johnson SM (2000) Respiratory rhythm generation in neonatal and adult mammals: the hybrid pacemaker-network model. Respir Physiol 122: 131–147

Solomon IC (2002) Modulation of gasp frequency by activation of pre-Bötzinger complex in vivo. J Neurophysiol 87: 1664–1668

Solomon, IC, Edelman NH, Neubauer JA (2000) Pre-Bötzinger complex functions as a central hypoxia chemosensor for respiration in vivo. J Neurophysiol 83: 2854–2868

Song JH, Huang CS, Nagata K, Yeh JZ, Narahashi T (1997) Differential action of riluzole on tetrodotoxin-sensitive and tetrodotoxin-resistant sodium channels. J Pharmacol Exp Ther 282: 707–714

St John WM, Paton JFR (2002) Neurogenesis of gasping does not require inhibitory transmission using $GABA_A$ or glycine receptors. Respir Physiol Neurobiol 132: 265–277

St-John WM, Rybak IA, Paton JFR (2002) Potential switch from eupnoea to fictive gasping after blockade of glycine transmission and potassium channels. Am J Physiol Integr Comp Physiol 283: R721–R731

Takakusaki K, Kitai ST (1997) Ionic mechanisms involved in the spontaneous firing of tegmental pedunculopontine nucleus neurons of the rat. Neurosci 78: 771–794

Thoby-Brisson M, Ramirez JM (2001) Identification of two types of inspiratory pacemaker neurons in the isolated respiratory network of mice. J Neurophysiol 86: 104–112

Thompson RJ, Nurse CA (1998) Anoxia differentially modulates multiple $K+$ currents and depolarizes neonatal rat adrenal chromaffin cells. J Physiol Lond 512: 421–434

Von Euler C (1986) Brainstem mechanism for generation and control of breathing pattern. In: Chernack NS, Widdicombe JG (eds) Handbook of physiology. The respiratory system II. American Physiology Society, Bethesda, MD, pp 1–67

Zheng Y, Riche D, Rekling JC, Foutz AS, Denavit-Saubie M (1998) Brainstem neurons projecting to the rostral ventral respiratory group (VRG) in the medulla oblongata of the rat revealed by co-application of NMDA and biocytin. Brain Res 782: 113–125